Vietnam Journal of Science and Technology ***63*** *(2) (2025) 402-415*
doi:10.15625/2525-2518/20303

Optimization of third-order trajectory to reduce the vibration in a point-to-point motion system

Rupesh Tatte*, Hemant Jawale, Hemant Thorat

Department of Mechanical Engineering, Visvesvaraya National Institute of Technology, 43F2+7JR, S Ambazari Rd, Ambazari, Nagpur, 440010, India

*Emails: *rupeshtatte0096@gmail.com*

Received: 10 March 2024; Accepted for publication: 6 May 2024

Abstract. In point-to-point motion transfer applications, where motion is executed from one point to another along a pre-planned path with high speed and precision, the occurrence of vibration is a common problem. This problem is addressed through motion profile planning, where an S-curve motion profile is reported to produce lesser vibration than a trapezoidal velocity profile. This paper introduces an optimization method designed to optimize a polynomial-function-based 7-segment third-order symmetrical (7-STOS) S-curve motion profile to minimize vibration. The method aims to achieve lower vibration amplitude for a given distance travelled and motion time (MT) without considering the dynamics of the system. The optimization method is developed using a novel unitization and the weighted sum approach. The effectiveness of the proposed method is demonstrated using an experimental setup of a flexible rotating link. The modelling of flexible rotating links is provided to facilitate the validation of experimental results with simulated results.

Keywords: Motion profile, motion parameters, motion time, weights

Classification numbers: 5.3.6, 5.4.2, 5.6.2.

1. INTRODUCTION

In speedy and highly precised motion transfer systems such as robots, computer numerical control (CNC) machines, etc., point-to-point motion is extensively employed. This type of motion aims to be accomplished either in the minimum possible time or within a specific time frame. Achieving point-to-point motion requires trajectory planning involving a control algorithm created using motion profiles. The trapezoidal velocity or second-order motion profile is capable of delivering fast motion. However, this profile generates infinite jerk, leading to significant jerk forces that induce vibrations [1]. Therefore, the S-curve motion profiles are introduced which gives an smoother and controlled optimum trajectory [2 - 5].

In recent years, lots of work have been carried out to control the vibration using an S-curve motion profile [6 - 8]. Lee *et al.* present a fuzzy system that works on the S-curve switching method. The method aids in designing the third-order S-curve motion profile by predicting a new maximum velocity reducing the vibration due to uncertain load [9]. A time-optimum third-

order S-curve trajectory is designed by optimizing the ramp-up time to reduce the residual vibration [10]. A parameter, jerk ratio, is introduced to design a third-order asymmetrical S-curve (AS-curve) motion profile for reducing the induced residual vibration in the flexible motion system [11 - 15]. In another work, a speedy acceleration and slow deceleration third-order AS-curve motion profile is presented for obtaining the expected position with a minimum residual vibration [16 - 18]. A look-ahead algorithm is presented to design a third-order AS-curve motion profile [19]. The algorithm drastically lowered the machining time and smoothened the CNC machine's feed rates. A genetic algorithm is presented to design a third-order AS-curve motion profile for a five-axis machine tool [20]. The algorithm obtains higher machining speed without breaching the axes limiting values. Bai *et al.* introduce a freeform time-optimal third-order AS-curve motion profile to efficiently optimize both the phase terms and magnitude in residual vibration [21]. Lu *et al.* present a particle swarm optimization technique to optimize the end velocity of the third-order AS-curve motion profile for achieving smooth and fast motion [22]. Lambrechts *et al.* and Fan *et al.* present an optimization algorithm to design the time-optimum S-curve motion profiles to reduce the vibration [23, 24]. Lee and Ha present a new optimization algorithm to optimize S-curve motion profiles to obtain fast motion with lower residual vibration [25]. Numerous studies have been conducted on optimizing S-curve motion profiles to minimize vibration. However, most of these studies typically offer an optimal time solution without addressing specific time requirements, and they often fail to produce the optimum trajectory without considering system dynamics.

In this paper, an optimization method is presented to design the optimum 7-STOS S-curve motion profile for achieving low vibration response. The optimization method enables the attainment of low vibration response for a specific motion time (MT) and distance travelled without considering the system dynamics. An optimization method is developed using a novel unitization and the weighted sum approach. Four optimum 7-STOS S-curve motion profiles are obtained by prioritizing each motion parameter individually and considering all motion parameters. Among these optimum motion profiles, the global optimum 7-STOS S-curve motion profile is the one that produces the low vibration response. The efficacy of the presented method is experimentally demonstrated on the setup of a flexible rotating link. The modelling of flexible rotating links is given to facilitate the validation of experimental results with simulated results.

The remaining sections of this paper are organized as follows: Section 2 outlines the methodology for generating a 7-STOS S-curve motion profile. Section 3 discusses the optimization of a unitized 7-STOS S-curve motion profile. Experimental validation of the proposed optimization method is presented in Section 4. Finally, conclusions are drawn in Section 5.

2. THIRD-ORDER TRAJECTORY PLANNING

The third-order S-curve motion profile discussed in this study is a 7-STOS S-curve motion profile designed for point-to-point motion. Figure 1 illustrates a schematic view of 7-STOS S-curve motion profile, comprising jerk, acceleration, velocity, and displacement profiles. Δt_j, Δt_a, and Δt_v represent the time durations of uniform jerk, uniform acceleration, and uniform velocity, respectively. The profile consists of four Δt_j segments, two Δt_a segments, and one Δt_v segment, giving the MT as $\Delta t = 4\Delta t_j + 2\Delta t_a + \Delta t_v$.

This motion profile can be segmented into three main periods: acceleration from [0, $2\Delta t_j+\Delta t_a$], uniform velocity from [$2\Delta t_j+\Delta t_a$, $2\Delta t_j+\Delta t_a+\Delta t_v$] and retardation from [$2\Delta t_j+\Delta t_a+\Delta t_v$, $4\Delta t_j+2\Delta t_a+\Delta t_v$]. The acceleration and retardation phases can be further divided into three sub-

periods. The maximum magnitudes reached by displacement, velocity, acceleration, and jerk are represented by *d*, *v*, *a*, and *j*, respectively.

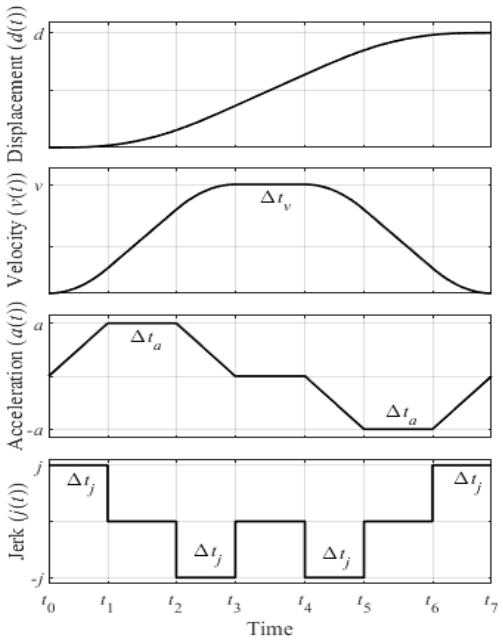

Figure 1. 7-STOS S-curve motion profile.

The jerk profile of the 7-STOS S-curve motion profile is expressed by the equations provided in Eqn. (1). The profile is determined for each time segment with variables a and Δt_j.

$$j(t)=\begin{cases} \dfrac{a}{\Delta t_j} & 0\le t\le \Delta t_j,\ (3\Delta t_j+2\Delta t_a+\Delta t_v)\le t\le (4\Delta t_j+2\Delta t_a+\Delta t_v), \\ 0 & \Delta t_j\le t\le (\Delta t_j+\Delta t_a),\ (2\Delta t_j+\Delta t_a)\le t\le (2\Delta t_j+\Delta t_a+\Delta t_v) \\ & (3\Delta t_j+\Delta t_a+\Delta t_v)\le t\le (3\Delta t_j+2\Delta t_a+\Delta t_v) \\ -\dfrac{a}{\Delta t_j} & (\Delta t_j+\Delta t_a)\le t\le (2\Delta t_j+\Delta t_a), \\ & (2\Delta t_j+\Delta t_a+\Delta t_v)\le t\le (3\Delta t_j+\Delta t_a+\Delta t_v) \end{cases} \quad (1)$$

where $j(t)$ represents jerk for any given time.

The equations needed to determine the acceleration profile $a(t)$, velocity profile $v(t)$, and displacement profile $d(t)$ can be obtained by integrating Eqn. (1) once, twice, and thrice, respectively, with respect to time.

Unitization of 7-STOS S-curve motion profile

A novel unitization method is presented to generalize the work. This method aims to generalize the work by considering displacement and time as one unit each ($d = \Delta t = 1$). The resulting 7-STOS S-curve motion profile obtained by this method is called a unitized 7-STOS S-curve motion profile. The magnitudes of the motion parameters in the unitized 7-STOS S-curve motion profile are termed as unitized magnitudes. The unitized magnitudes of motion parameters

can be easily converted into actual magnitudes by multiplying them by the multiplication factor (MUF) provided in Table 1, where G_1 represents actual displacement and G_2 represents actual time to achieve G_1 displacement.

Table 1. MUF to achieve actual magnitudes.

Motion parameters	Velocity	Acceleration	Jerk
MUF	$\frac{G_1}{G_2}$	$\frac{G_1}{{G_2}^2}$	$\frac{G_1}{{G_2}^3}$

Table 2. Minimum possible peak magnitudes and corresponding other magnitudes of various motion parameters.

	Motion profile	Uniform velocity	Uniform acceleration	Uniform jerk
	Motion parameters	v	a	j
	Minimum possible peak magnitudes	1	4	32
Corresponding other peak magnitudes for minimum possible magnitude condition of the motion parameters	v	1	2	2
	a	∞	4	8
	j	∞	∞	32
Corresponding time durations of segments	Δt_j	0	0	0.25
	Δt_a	0	0.5	0
	Δt_v	1	0	0

The 7-STOS S-curve motion profile is further examined by managing the values of Δt_v, Δt_a, and Δt_j under the condition that $4\Delta t_j + 2\Delta t_a + \Delta t_v = 1$. Conventional uniform velocity, uniform acceleration, and uniform jerk motion profiles are special cases of the 7-STOS S-curve motion profile. These conventional motion profiles provide the minimum possible peak magnitudes of motion parameters. The peak magnitudes and values of Δt_v, Δt_a, and Δt_j for $d = \Delta t = 1$ are provided for reference in Table 2. For these minimum possible peak magnitudes, the other motion parameter's magnitudes are also given in Table 2.

3. OPTIMIZATION OF UNITIZED 7-STOS S-CURVE MOTION PROFILE

Minimizing the magnitudes of more than two parameters simultaneously is more challenging than minimizing the magnitudes of one or two parameters. Optimization method is crucial for optimizing the magnitudes of motion parameters. An optimization function is developed and presented to provide an appropriate solution that regulates the magnitudes of motion parameters according to the assigned weights. A multi-objective optimization function is formulated for optimizing the magnitudes of motion parameters. This function uses the weighted sum technique to transform the multi-objective problem by creating a weighted sum of all the objective functions. The technique allows for the prioritization of specific motion parameters.

The objective functions are formulated to ensure that minimizing the motion parameter's magnitude results in the minimum value, while maximizing it yields the maximum value. Given that the maximum possible magnitudes a and j can extend to infinity (∞), for extracting a near-

optimal solution, the ideal range for each objective function is from a finite value to ∞. Consequently, the objective functions are generated for the range between one to ∞. The formulated multi-objective optimization function is presented as follows:

$$\text{minimize } f(\bar{t}) = \sum_{i=v}^{s} W_i R_i(\bar{t}) = W_v R_v(\bar{t}) + W_a R_a(\bar{t}) + W_j R_j(\bar{t})$$

$$\text{minimize } f(\bar{t}) = W_v \left(\frac{1}{2\text{-}v}\right) + W_a \left(\frac{a}{4}\right) + W_j \left(\frac{j}{32}\right) \tag{2}$$

$$\text{Subject to} \quad 1 \le R_v(\bar{t}) / R_a(\bar{t}) / R_j(\bar{t}) \le \infty$$

where, $\bar{t} = \left(\Delta t_a, \Delta t_j\right)^{\mathrm{T}}$ is the vector of decision variables. The lower and upper bounds of the decision variables are 0 and 0.5 for Δt_a and 0 and 0.25 for Δt_j. The scalar weights W_v, W_a, and W_j are belonging to the objective function of velocity $R_v(\bar{t})$, acceleration $R_a(\bar{t})$, and jerk $R_j(\bar{t})$, respectively. The scalar weights should be set such that $W_i \geq 0$ [26]. It is not necessary to impose any restrictions on the weight's values, such as $\sum_{i=v}^{s} W_i = 1$, other than $W_i \geq 0$, which guarantees an optimum solution [26].

The v, a, and j are the functions of two decision variables, i.e., Δt_a and Δt_j, and their equations are given as follows:

$$j = -\frac{1}{\left(\Delta t_j\left(\Delta t_j + \Delta t_a\right)\left(2\Delta t_j - 1 + \Delta t_a\right)\right)} \tag{3}$$

$$a = -\frac{-\Delta t_j}{\left(\Delta t_j\left(\Delta t_j + \Delta t_a\right)\left(2\Delta t_j - 1 + \Delta t_a\right)\right)} \tag{4}$$

$$v = -\frac{1}{\left(2\Delta t_j - 1 + \Delta t_a\right)} \tag{5}$$

Determination of unitized optimum magnitudes

The relative importance of a specific motion parameter varies across different point-to-point motion transfer applications, serving as a basis for the selection of weights. Therefore, the optimum motion profiles are obtained by preferring a specific motion parameter while simultaneously considering all of the motion parameters. The unitized optimum magnitudes are obtained for four different combinations of relative weights or four different cases. The optimum magnitudes for the first case are obtained by assigning equal weights to the motion parameters, i.e., $W_v = W_a = W_j = 1$. The optimum magnitudes for the second case are obtained by assigning more weight to velocity ($W_v = 10$) and lower weight to acceleration and jerk. The optimum magnitudes for the third case are obtained by assigning more weight to acceleration (W_a=10) and lower weight to velocity and jerk. Finally, the optimum magnitudes for the fourth case are obtained by assigning more weight to jerk ($W_j = 10$) and lower weight to velocity and acceleration ($W_v = W_a = 1$). The unitized optimum magnitudes of motion parameters determined using the presented optimization method are given in Table 3. The unitized optimum 7-STOS S-curve motion profiles for first and second case are shown in Figure 2. It is observed that the motion parameters with higher weight have a magnitude very close to their minimum possible magnitudes.

The found optimum solutions are suitable for any point-to-point applications aiming to reduce vibration and provide smoothness in motion. It is crucial to identify the preferred motion

parameter among velocity, acceleration, and jerk. However, determining the preferred motion parameter is challenging due to the involvement of numerous calculations and complex mathematics related to system dynamics. To avoid the complexities of system dynamics and numerous calculations, it is necessary to use all of the optimum solutions. The best optimum or global optimum solution is the one that produces the lowest vibration amplitude.

Table 3. Unitized optimum magnitudes of motion parameters according to the given preference.

Weights $(W_v/W_a/W_j)$	v	a	j
1/1/1	1.52	6.73	57.64
10/1/1	1.29	9.16	108.9
1/10/1	1.64	4.95	84.46
1/1/10	1.72	7.66	39.34

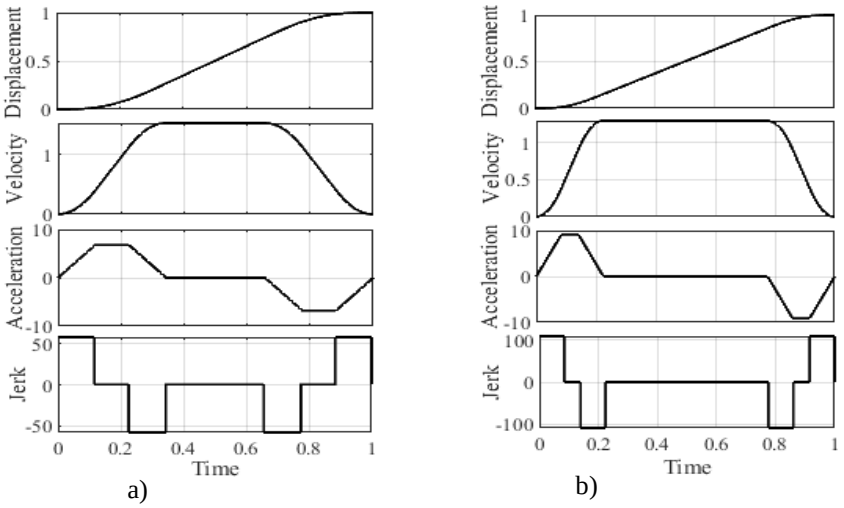

Figure 2. Unitized optimum 7-STOS S-curve motion profile for: (a) 1/1/1, (b) 10/1/1, (c) 1/10/1, and (d) 1/1/10 weighting combinations.

4. VALIDATION

A flexible rotating link is employed to showcase the efficacy of the presented optimization method. Such a system is capable of causing residual vibration both during and after the completion of the point-to-point motion. The main goal is to minimize the vibration at the end of the point-to-point motion.

4.1. Theoretical background

The flexible rotating link discussed here can be regarded as an Euler-Bernoulli beam. The model of this flexible rotating link is depicted in Figure 3. A dynamic model is formulated to extract the vibration response using Lagrange's equation. In the equation, the link parameters m_t, m, and l, denote the mass attached at the free end of the link, the uniform weight per unit length of the link, and the length of the link, respectively. The angle of the hub is denoted by $\theta(t)$. The

flexible rotating link's deflection ($w(l,t)$) concerning time at a distance l is given by an assumed mode method.

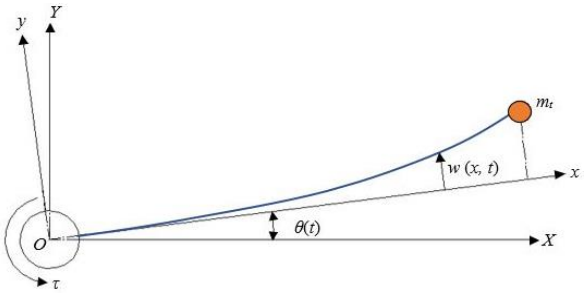

Figure 3. Flexible rotating link.

The simplified transfer function for deflection $w(l,t)$, relative velocity $\dot{w}(l,t)$, and relative acceleration $\ddot{w}(l,t)$ at the tip end ($x = l$) is given as follows:

$$\frac{w(s)}{\theta(s)} = \frac{\dot{w}(s)}{\dot{\theta}(s)} = \frac{\ddot{w}(s)}{\ddot{\theta}(s)} = \frac{-m_1 \Psi(l) s^2}{m_2 s^2 + cs + k} \tag{6}$$

where $\theta(s), \dot{\theta}(s), \ddot{\theta}(s), w(s), \dot{w}(s)$ and $\ddot{w}(s)$ are the Laplace forms of $d(t)$, $v(t)$, $a(t)$, $\ddot{w}(l,t)$, $\dot{w}(l,t)$, and $\ddot{w}(l,t)$, respectively. The damping coefficient is denoted by c, k is the stiffness factor of the link ($k = m\omega^2$, ω is the dominant natural frequency of the link) and $\Psi(l)$ is the normalized mode shape for the fixed-free boundary condition at a distance l.

$$m_1 = m \int_0^1 \Psi(x) x \, dx + m_t l \Psi(l) \tag{7}$$

$$m_2 = m + m_t \Psi^2(l) \tag{8}$$

The solution to the homogeneous eigenvalue problem for the normalized mode shape under the fixed-free boundary condition is expressed as follows [27]:

$$\Psi(l) = \frac{l}{e} [\cosh \gamma - \cos \gamma + \beta(\sin \gamma - \sinh \gamma)] \tag{9}$$

where e and β is given as

$$e = \left[l + \frac{ml^2}{m_t \gamma^2} \left(\frac{1 + \cosh(\gamma) \cos(\gamma)}{\sinh(\gamma) \sin(\gamma)} \right)^2 \right]^{\frac{1}{2}} \tag{10}$$

$$\beta = \frac{\cosh(\gamma) + \cos(\gamma)}{\sinh(\gamma) + \sin(\gamma)} \tag{11}$$

γ is the eigenvalue which can be calculated using the following characteristics equation of the fixed-free boundary condition.

$$1 + \frac{m_t \gamma}{ml} [\sinh(\gamma) \cos(\gamma) - \cosh(\gamma) \sin(\gamma)] + \cosh(\gamma) \cos(\gamma) = 0. \tag{12}$$

4.2. Experimentation

An experiment is performed on the flexible rotating link to validate the efficacy of the presented optimization method. Figure 4 depicts the experimental setup of the flexible rotating link. The flexible link is connected perpendicular to the motor shaft via a rotating hub. To measure the tip-end vibration, an accelerometer is positioned at the tip-end of the flexible link. The experiments are conducted for two different flexibilities of the link. A mass of m_t = 0.02 kg is also affixed at the tip-end of the flexible link. The damping coefficient and length of the links are c = 0.15 N-sec/m and l = 0.295 m. The natural frequencies of the 1st and 2nd flexible links are ω_1 = 3.5 Hz and ω_2 = 5.7 Hz. The uniform weight per unit length of the 1st and 2nd links are m_1 = 0.125 kg/m and m_2 = 0.18 kg/m. The target moving distance is set at 100 degrees, i.e., 1.745 rad. The maximum velocity (v_{max} = 6 rad/sec), maximum acceleration (a_{max} = 50 rad/sec^2), and maximum jerk (j_{max} = 1500 rad/sec^3) are obtained by the capacity of the motor. A Teensy 3.6 microcontroller is utilized as a signal generator to produce 15 kHz and 12-bit PWM driving voltage signals at a 250 μs sampling rate.

For a given value of actuator limitations (v_{max}, a_{max}, j_{max}), the minimum MT for the 7-STOS S-curve motion profile is computed as 0.474 sec [23]. The experiments are conducted with three different MT values, i.e., 0.6 sec, 0.8 sec, and 1 sec.

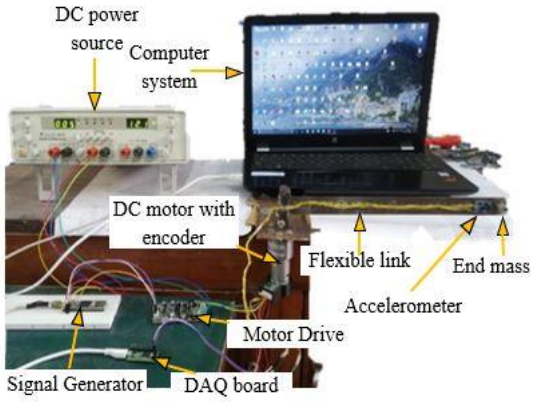

Figure 4. Experimental setup of flexible rotating link.

Before conducting the experiments, it is necessary to determine the MUF for a given value of MT and targeted distance. The MUF for velocity (MUF_v), acceleration (MUF_a), and jerk (MUF_j) are computed according to Table 1, and they are listed in Table 4. The actual optimum magnitudes of the motion parameters are calculated by multiplying the unitized optimum magnitudes given in Table 3 with the MUF given in Table 4. The actual optimum magnitudes of motion parameters for three different MT values are given in Table 5. The experiments are then performed utilizing all of the optimum 7-STOS S-curve motion profiles. The global optimum 7-STOS S-curve motion profile will be the one that gives the minimum vibration amplitude.

Table 4. MUF for different MTs.

MUF	MT (sec)		
	0.6	0.8	1
MUF_v	2.908	2.181	1.745
MUF_a	4.847	2.726	1.745
MUF_j	8.079	3.408	1.745

The experiments are performed with two various natural frequencies of the flexible links across three different MT. The experimentally obtained vibration amplitude at the tip-end of the flexible links just at the end of the motion is shown in Figure 5. In Figure 5, two figures are plotted: one for the 1st link and the other for the 2nd link. In each figure, the vibration amplitude for the four different combinations of relative weights is plotted across different MT. In these two figures of Figure 5, the lower amplitude observed for a given MT is the minimum vibration amplitude for that MT. The same minimum vibration amplitudes for both links with respect to the given MT are plotted in Figure 6.

Table 5. Actual optimum magnitudes of motion parameters for different MTs.

Weightages ($W_v/W_a/W_j$)	Motion Parameter	MT		
		0.6 sec	0.8 sec	1 sec
1/1/1	v (rad/sec)	4.42	3.31	2.65
	a (rad/sec^2)	32.62	18.34	11.74
	j (rad/sec^3)	465.67	196.44	100.58
10/1/1	v (rad/sec)	3.75	2.81	2.25
	a (rad/sec^2)	44.39	24.97	15.98
	j (rad/sec^3)	879.8	371.13	190
1/10/1	v (rad/sec)	4.77	3.58	2.86
	a (rad/sec^2)	24	13.49	8.64
	j (rad/sec^3)	682.35	287.84	147.38
1/1/10	v (rad/sec)	5	3.75	3
	a (rad/sec^2)	37.13	20.88	13.37
	j (rad/sec^3)	317.83	134.07	68.65

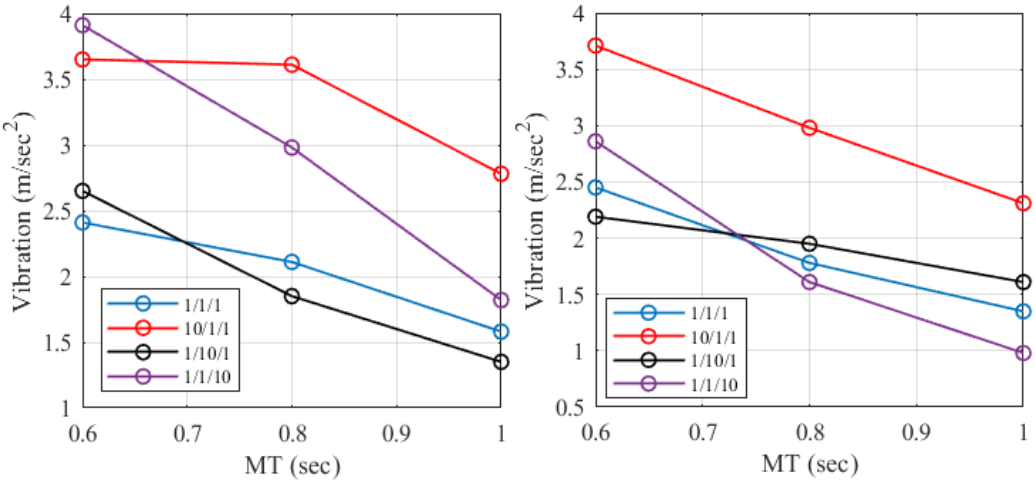

Figure 5. Vibration amplitude for (a) 1st link and (b) 2nd link.

For 0.6 sec MT, the optimum motion profile with 1/1/1 and 1/10/1 weighting values produces the minimum vibration amplitude for 1st and 2nd links, respectively. For 0.8 sec MT, the optimum motion profile with 1/10/1 and 1/1/10 weighting value produces the minimum vibration amplitude for 1st and 2nd links, respectively. For 1 sec MT, the optimum motion profile

with 1/10/1 and 1/1/10 weighting value produces the minimum vibration amplitude for 1st and 2nd links, respectively. For both 0.8 sec and 1 sec MT, the preference of weight shifts to the next derivative from acceleration in 1st link to jerk in 2nd link. The simulated results are generated using the same combination of relative weights that experimentally produce the minimum vibration amplitudes. These simulated results for the 1st and 2nd flexible links are plotted in Figure 6, alongside the experimental results for comparison. The experimental results are observed to agree well with the simulated results.

It is observed that there is no single combination of relative weights that can produce the minimum vibration amplitude for the 1st and 2nd links across different MT. Therefore, the variation in the vibration amplitude for each combination of relative weight is non-linear. There are some combinations, such as 1/1/10 for the 1st flexible link and 10/1/1 and 1/10/1 for the 2nd flexible link, where the vibration amplitude varies linearly.

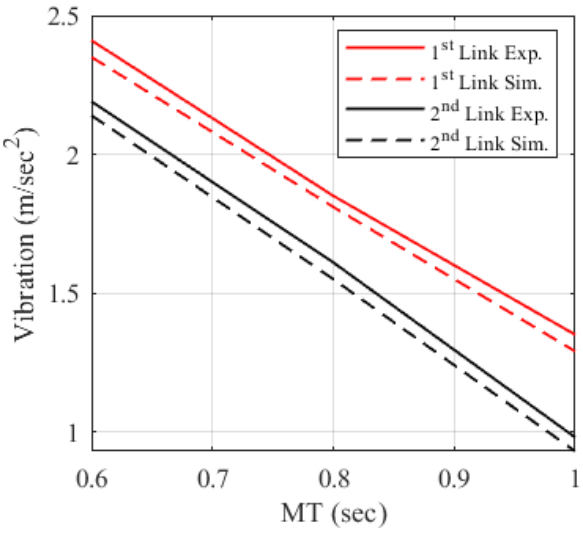

Figure 6. Comparison of simulated and experimentally obtained minimum vibration amplitude.

4.2.1. Performance comparison of motion profiles

The efficacy of the presented optimum 7-STOS S-curve motion profile is demonstrated in comparison with the conventional optimum 7-STOS S-curve motion profile. The time parameters for creating the conventional optimum motion profile are determined according to the given actuator limitations. The effectiveness is evaluated in the context of the capability of producing the lower vibration amplitude at the completion of the motion. The comparison of vibration amplitude between the proposed optimum and conventional optimum profile is shown in Table 6. The overall vibration response of 1st and 2nd flexible links for the conventional optimum and proposed optimum profiles are shown in Figure 7.

The proposed optimum profile produces lower vibration as compared to the conventional optimum profile. Although the MT for the conventional optimum profile is short, the profile does not produce a lower vibration amplitude. For a 0.6 sec MT, the proposed optimum profile reduces the vibration amplitude by 59.1 % for the 1st link, as shown in Figure 7(a), and 73 % for the 2nd link, as shown in Figure 7(b), as compared to the conventional optimum profile. Similarly, for 0.8 sec and 1 sec MT, the proposed optimum profile reduces the vibration

amplitude significantly by 68.6 % and 77.1 % for the 1st link, as shown in Figure 7(a), and 80.1 % and 88 % for the 2nd link, as shown in Figure 7(b), respectively, as compared to the conventional optimum profile.

Table 6. Comparison of vibration amplitude.

Motion Profile	Link	MT (sec)	Vibration Amplitude (m/sec^2)
Conventional Optimum 7-STOS S-curve Motion Profile	1st	0.474	5.89
	2nd		8.1
Proposed Optimum 7-STOS S-curve Motion Profile	1st	0.6	2.41
	2nd		2.19
	1st	0.8	1.85
	2nd		1.61
	1st	1	1.35
	2nd		0.98

The proposed optimum 7-STOS S-curve motion profile is capable of producing lower vibration amplitude without any knowledge of the system's parameters, which eliminates the need for intricate mathematics and computational work. Consequently, the proposed 7-STOS S-curve motion profile can effectively suppress the vibration amplitude for any specific MT and distance travelled.

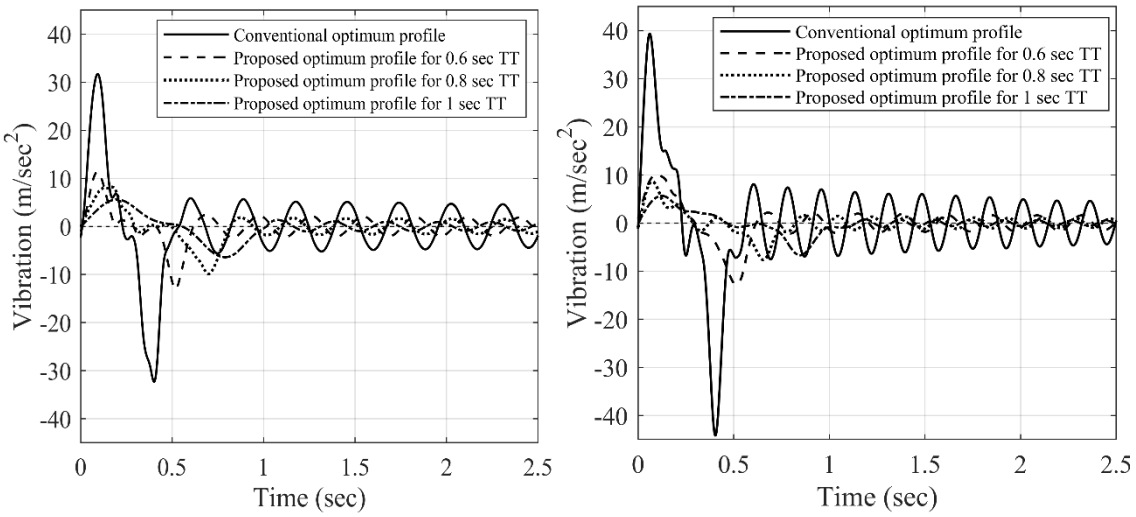

Figure 7. Comparison of minimum vibration response between conventional and proposed optimum profile: (a) 1st flexible link, (b) 2nd flexible link.

5. CONCLUSIONS

The paper presents an optimization method to design an optimum 7-STOS S-curve motion profile for achieving low vibration response. The proposed optimization method produces a minimum vibration response for a specific MT and distance travelled without accounting for system dynamics. The unitization approach introduced in this paper allows the generalization of designing a 7-STOS S-curve profile for specific MT and distance travelled. The four different optimum 7-STOS S-curve motion profiles are designed in accordance with the preference given to the motion parameters. The designed optimum profiles can be applied to any point-to-point motion transfer application for reducing vibration. The practicality of the presented optimum 7-STOS S-curve motion profile is demonstrated using the experimental setup of a flexible rotating link. The experiments are performed for all of the four optimum profiles. Only four experiments are required to be performed to achieve low vibration response, and it can be achieved without entering into any complex mathematics related to the system dynamics. The performance of the presented method is verified by comparing it with the conventional method. It is found that the proposed method reduces vibration more effectively as compared to the conventional method.

Acknowledgement. This research is not financially supported by any organization. The author would like to express gratitude to Visvesvaraya National Institute of Technology, Nagpur, for their valuable support and insightful discussions throughout this research. Additionally, we sincerely appreciate the constructive feedback from the reviewers, which has helped improve the quality of this work.

CRediT authorship contribution statement. Rupesh Tatte: Methodology, Investigation. Hemant Thorat: Formal analysis, Supervision. Hemant Jawale: Formal analysis, Supervision.

Declaration of competing interest. The authors declare that they have no known competing financial interests or personal relationships that could have appeared to influence the work reported in this paper.

REFERENCES

1. Li H., Le M. D., Gong Z. M., Lin W. - Motion profile design to reduce residual vibration of high-speed positioning stages, IEEE/ASME Trans. Mechatronics **14** (2009) 264-269. https://doi.org/10.1109/TMECH.2008.2012160
2. Li H. Z., Gong Z. M., Lin W., Lippa T. - Motion profile planning for reduced jerk and vibration residuals, SIM Tech. **8** (2015) 32-37. https://doi.org/10.13140/2.1.4211.2647
3. Perumaal S., Jawahar N. - Synchronized trigonometric S-curve trajectory for jerk-bounded time-optimal pick and place operation, Int. J. Robot. Autom. **27** (2012) 385-395. https://doi.org/10.2316/Journal.206.2012.4.206-3780
4. Nguyen K. D., Ng T. C., Chen I. M. - On algorithms for planning s-curve motion profiles, Int. J. Adv. Robot. Syst. **5** (2008) 99-106. https://doi.org/10.5772/5652
5. Ouyang H., Hu J., Zhang G., Mei L., Deng X. - Decoupled linear model and S-shaped curve motion trajectory for load sway reduction control in overhead cranes with double-pendulum effect, Proc. Inst. Mech. Eng. Part C J. Mech. Eng. Sci. **233** (2019) 3678-3689. https://doi.org/10.1177/0954406218819029
6. Ding H., Member S., Wu J. - Point-to-point motion control for a high-acceleration positioning table via cascaded learning schemes, IEEE Trans. Ind. Electron. **54** (2007) 2735-2744. https://doi.org/10.1109/TIE.2007.894702
7. Erkorkmaz K., Altintas Y. - High speed CNC system design . Part I : jerk limited trajectory generation and quintic spline interpolation, Int. J. Mach. Tools. Manuf. **6955**

(2001) 2-5. https://doi.org/10.1016/S0890-6955(01)00002-5

8. Garcia Martinez J. R., Rodriguez Resendiz J., Martinez Prado M. A., Cruz Miguel E. E. - Assessment of jerk performance s-curve and trapezoidal velocity profiles, 13th Int. Eng. Congr. (2017). https://doi.org/10.1109/CONIIN.2017.7968187
9. Lee S. Y., Kang C. S., Hyun C. H., Park M. - S-curve profile switching method using fuzzy system for position control of DC motor under uncertain load, Int. Conf. Control Autom. Syst. (2012) 91-95.
10. Meckl P. H., Arestides P. B., Woods M. C. - Optimized S-curve motion profiles for minimum residual vibration, Proc. Am. Control Conf. **5** (1998) 2627-2631. https://doi.org/10.1109/ACC.1998.688324
11. Rew K. H., Kim K. S. - A closed-form solution to asymmetric motion profile allowing acceleration manipulation, IEEE Trans. Ind. Electron. **57** (2010) 2499-2506. https://doi.org/10.1109/TIE.2009.2036032
12. Ha C. W., Rew K. H., Kim K. S. - A complete solution to asymmetric S-curve motion profile: Theory & experiments, Int. Conf. Control Autom. Syst. (2008) 2845-2849. https://doi.org/10.1109/ICCAS.2008.4694244
13. Rew K. H., Kim K. S. - Using asymmetric S-curve profile for fast and vibrationless motion, Int. Conf. Control Autom. Syst. (2007) 500-504. https://doi.org/10.1109/ICCAS.2007.4406961
14. Rew K. H., Ha C. W., Kim K. S. - A practically efficient method for motion control based on asymmetric velocity profile, Int. J. Mach. Tools Manuf. **49** (2009) 678-682. https://doi.org/10.1016/j.ijmachtools.2009.01.008
15. Ha C. W., Rew K. H., Kim K. S. - Robust zero placement for motion control of lightly damped systems, IEEE Trans. Ind. Electron. **60** (2013) 3857-3864. https://doi.org/10.1109/TIE.2012.2206334
16. Tsay D. M., Lin C. F. - Asymmetrical inputs for minimizing residual response, IEEE Int. Conf. Mechatronics (2005) 235-240. https://doi.org/10.1109/ICMECH.2005.1529259
17. Zou F., Qu D., Xu F. - Asymmetric s-curve trajectory planning for robot point-to-point motion, IEEE Int. Conf. Robot Biomimetics (2009) 2172-2176. https://doi.org/10.1109/ROBIO.2009.5420482
18. Bearee R., Olabi A. - Dissociated jerk-limited trajectory applied to time-varying vibration reduction, Robot Comput. Integr. Manuf. **29** (2013) 444-453. https://doi.org/10.1016/j.rcim.2012.09.014
19. Chen Y., Ji X., Tao Y., Wei H. - Look-ahead algorithm with whole s-curve acceleration and deceleration, Adv. Mech. Eng. **5** (2013) 1-9. https://doi.org/10.1155/2013/974152
20. Lu T. C., Chen S. L. - Genetic algorithm-based S-curve acceleration and deceleration for five-axis machine tools, Int. J. Adv. Manuf. Technol. **87** (2016) 219-232. https://doi.org/10.1007/s00170-016-8464-0
21. Bai Y., Chen X., Sun H., Yang Z. - Time-optimal freeform s-curve profile under positioning error and robustness constraints. IEEE/ASME Trans, Mechatronics **23** (2018) 1993-2003. https://doi.org/10.1109/TMECH.2018.2835830
22. Lu T. C., Chen S. L., Yang E. C. Y. - Near time-optimal s-curve velocity planning for multiple line segments under axis constraints, IEEE Trans. Ind. Electron. **65** (2018) 9582-9592. https://doi.org/10.1109/TIE.2018.2818669
23. Lambrechts P., Boerlage M., Steinbuch M. - Trajectory planning and feedforward design for electromechanical motion systems, Control Eng. Pract. **13** (2005) 145-157.

https://doi.org/10.1016/j.conengprac.2004.02.010

24. Fan W., Gao X. S., Yan W., Yuan C. M. - Interpolation of parametric CNC machining path under confined jounce, Int. J. Adv. Manuf. Technol. **62** (2012) 719-739. https://doi.org/10.1007/s00170-011-3842-0
25. Lee D., Ha C. W. - Optimization process for polynomial motion profiles to achieve fast movement with low vibration. IEEE Trans, Control Syst. Technol. **28** (2020) 1892-1901. https://doi.org/10.1109/TCST.2020.2998094
26. Marler R. T., Arora J. S. - The weighted sum method for multi-objective optimization: New insights, Struct. Multidiscip. Optim. **41** (2010) 853-862. https://doi.org/10.1007/s00158-009-0460-7
27. Model S., Sun C., He W., Member S., Hong J., Member S. - Neural network control of a flexible robotic manipulator using the lumped spring-mass model, IEEE Trans. Syst. Man. Cybern. **47** (2016) 1-12. https://doi.org/10.1109/TSMC.2016.2562506.